


Chirality Hot Paper


A Chiral-Label-Free SERS Strategy for the Synchronous Chiral Discrimination and Identification of Small Aromatic Molecules

Yue Wang,* Xueqi Zhao, Zhi Yu,* Zhangrun Xu, Bing Zhao, and Yukihiro Ozaki*

Abstract: A versatile and robust chiral discrimination strategy for small aromatic compounds is of significant importance in multidisciplinary fields. However, most current methods lack either the sufficient sensitivity for recognizing the chirality of the target molecules or their molecular specificity information. We have developed a versatile and chiral-label-free surface-enhanced Raman scattering (SERS)-based chiral discrimination sensing system for small aromatic molecules, where the molecular structural specificity and enantioselectivity can be given synchronously in a single SERS spectrum. More than 10 types of chiral aromatic molecules were successfully identified by using this system. This work has enormous potential for recognizing chiral products effectively in sophisticated systems, especially in the fields of chiral synthesis and chiral catalysis.

Introduction

Chirality is one of the remarkable features in nature because a variety of molecular building blocks show intrinsic chiral preference and strict chiral selectivity, which has been the significant issue plaguing researchers exploring the origins of life.^[1–3] The enantiomers of a chiral molecule are stereoisomers that are non-superimposable mirror images of each other.^[4] Despite the similar physical and chemical properties between them, they exhibit entirely different physiological effects in terms of biological activities, toxicities, and pharmacological actions. Chiral discrimination, the distinction

How to cite: *Angew. Chem. Int. Ed.* **2020**, *59*, 19079–19086
 International Edition: doi.org/10.1002/anie.202007771
 German Edition: doi.org/10.1002/ange.202007771

between left- and right-handed enantiomers, has aroused considerable interest due to its pivotal importance not only in chemistry, biology, and pharmacology, but also in daily life.^[5] Chiral aromatic molecules, such as some amino acids, are important molecular units of numerous biological substances, and are also commonly used as chiral auxiliaries in industrial applications, such as natural product synthesis, chiral pharmaceutical synthesis, and asymmetrical catalysis.^[6,7] Thus, developing a sensitive and accessible chiral recognition and identification strategy, especially for chiral aromatic compounds, is extremely intriguing and challenging.

Many developments in chiral discrimination have been achieved through various techniques,^[8–15] which can be divided into two major categories based on different recognition mechanisms. Methods within the first category rely on the inherent optical activities of chiral molecules,^[9,10] where circularly polarized light is the prerequisite to distinguish between the two enantiomers. The other methods primarily depend on traditional lock-and-key molecular recognition, where specific chiral chemosensors are necessary to translate the chirality information of a target molecule by identifying stereostructure differences with the combination of a variety of methodologies, including chromatography,^[11] electrochemistry,^[11] colorimetry, and spectroscopy^[8,12] methods. In these discrimination systems, molecular chirality can be revealed by the preferential response of one enantiomer towards the other. Despite the establishment of diverse chiral discrimination approaches, the essential issue of current strategies is their strong dependency on chiral auxiliaries and circularly polarized light. Additionally, most of these present methods have left some crucial problem underlying chiral discrimination that is the poor recognition resolution and low sensitivity for various chiral targets. Regarding chiroptical sensing methodology, sufficient sensitivity and high recognition performance are usually absent. In the other case, only indirect recognition that is dependent on chiral chemosensors signals can be afforded by lock-and-key recognition approaches, which generally lack molecular specificity information of the chiral targets and are limited to only one or a few kinds of chiral molecules. Therefore, developing a straightforward and versatile chiral discrimination strategy that is chiral-label-free and possesses desirable identification capabilities has been a challenge yet attractive goal.


Surface-enhanced Raman scattering (SERS) spectroscopy, as a powerful technique with single-molecule-level sensitivity and high molecular fingerprint specificity, has been extensively applied to surface analysis and chemical identification in a wide range of fields, such as chemistry, biology, physics, and materials science.^[16,17] At present, two commonly accepted mechanisms are responsible for the tremendous

[*] Dr. Y. Wang, X. Zhao, Prof. Z. Yu
 Department of Chemistry, College of Sciences
 Northeastern University, Shenyang 110819 (P. R. China)
 E-mail: yuewang@mail.neu.edu.cn

Dr. Z. Yu
 State Key Laboratory of Applied Optics
 Changchun Institute of Optics, Fine Mechanics and Physics
 Chinese Academy of Sciences, Changchun 130033 (P. R. China)
 E-mail: zhiyu@ciomp.ac.cn

Prof. B. Zhao
 State Key Laboratory of Supramolecular Structure and Materials
 Jilin University
 2699 Qianjin Street, Changchun 130012 (P. R. China)

Prof. Y. Ozaki
 Department of Chemistry, School of Science and Technology,
 Kwansai Gakuin University
 Sanda, Hyogo 669-1337 (Japan)
 and
 Toyota Physical and Chemical Research Institute
 Nagakute, Aichi 480-1192 (Japan)
 E-mail: ozaki@kwansai.ac.jp

 Supporting information and the ORCID identification number(s) for the author(s) of this article can be found under:
<https://doi.org/10.1002/anie.202007771>.

SERS enhancement: the electromagnetic (EM) and the charge transfer (CT) mechanisms. The EM mechanism is derived from the dramatic local-field enhancement caused by localized surface plasmon resonance on a nanoscale metal substrate,^[18,19] and the CT mechanism is a short-range resonance-like process that is associated with the energy level structures between a substrate and the adsorbates.^[20,21] Although the EM mechanism is dominant in enhancing SERS signals, the CT mechanism is quite meaningful in that it offers information about electronic structure changes in a surface/interface system at the molecular level. Recently, CT-based SERS techniques have been demonstrated their superiority in exploring the effects of interfacial interactions.^[22,23] In terms of chiral discrimination, intermolecular interactions occur between each target enantiomer and an achiral recognition sensor, which alters the molecular electronic structures of the adsorbed sensor. Such changes are expected to be measured by CT-based SERS spectroscopy with evident differences in the spectral patterns between the two enantiomeric discrimination systems.^[15,24,25] As we previously reported, we first proposed a chiral-label-free chiral discrimination approach based on CT-SERS,^[15] which exhibited prominent advancement in its enantioselective discrimination response to several chiral alcohols without using any chiral sensor or circularly polarized light. Although we made progress in distinguishing between enantiomers by the impressive changes in the SERS spectra, the previous work has left much to be desired as a high discrimination sensitivity for low concentrations of the chiral targets was not achieved and that method did not work for detecting a wider range of chiral compounds except several chiral alcohols with low viscosity.^[15,25] The realization of chiral discrimination by SERS would satisfy the requirements for distinguishing between enantiomers and simultaneously identifying chiral molecules with higher sensitivity. These poor detectability problems could be overcome by a feasible SERS-based chiral discrimination approach with high sensitivity for identifying chiral targets that are dependent on EM mechanism and the specificity for reliable enantioselectivity that are related to the CT mechanism in the system. Thus, it is the key issue that we plan to solve by realizing synchronous chiral discrimination and molecular determination using the chiral-label-free discrimination sensing system presented in this work.

In this regard, appropriate sensors with sufficient interaction sites for enantioselective discrimination and molecular specificity should be the crucial component in this SERS-based discrimination system. Self-assembled monolayers (SAMs), especially thiol SAMs, are an essential system with remarkable structural features that have been extensively employed for modifying, protecting and functionalizing the surface of a material.^[26–28] Functionalized thiol SAMs on metal nanomaterials offer an accessible and effective way to tune the properties of the materials surface and be able to anchor the target molecules by intermolecular interactions or covalent bonding; therefore, they have widespread applications in many fields, such as catalysis, biosensing, corrosion protection, and organic electronics.^[29–31] Nevertheless, SAMs with single type of thiol on the surface of nanomaterials can merely implement rough control of the surface properties,

and the preferable tunability is limited.^[32,33] Modifying nanomaterial surfaces with mixed-thiol SAMs of two or more thiols has attracted more attentions, because the surface properties can be precisely adjusted by integrating the respective structural features of each type of thiol.^[28,32,33] It should be possible to achieve enantioselective discrimination and molecular fingerprint specificity detection by exploiting a SERS-active substrate modified with mixed-thiol SAMs. Well-controlled SERS-active substrates with remarkable enhancement are another essential consideration for a SERS-based discrimination method to improve the determination of chiral molecules. The self-assembled metal nanoparticles in ordered arrays exhibit dramatically high EM fields, affording SERS with enhanced optical signals.^[34,35] Vertically aligned Au nanorods (Au NRs) arrays, with great stability and optical tunability and have attracted significant attention since they possess remarkable collective plasmonic properties and engender intense localized EM fields with excellent spectral repeatability.^[36,37] In view of this, a vertically ordered Au NRs array as a SERS-active substrate in a chiral discrimination system is desirable and expected to improve spectral resolution for identifying molecular chirality and specificity.

Herein, we have proposed a versatile and chiral-label-free SERS-based chiral discrimination sensing system for small aromatic compounds, including chiral aromatic amines, alcohols, and acids, with high molecular fingerprint specificity, composed of mixed-thiol SAMs and vertically aligned Au NRs arrays. Two achiral thiols, *n*-hexanethiol (HT) and *p*-mercapto phenylboronic acid (MPBA), were selected to generate the functionalized SAMs in the chiral discrimination sensing system. The chiral aromatic targets are bound to the modified HT molecules by hydrophobic effects and weak intermolecular interactions, which place them in the vicinity of the hot spot regions on the surface of the Au NRs arrays to be facilely detected. In such a case, the trapped chiral molecules can be further recognized by the adjacent MPBA anchored to the Au NRs, where differences in the CT occur due to the different intermolecular hydrogen bonds between two enantiomeric systems. This leads to different SERS spectra of the MPBA, amplifying the difference in chirality. This work has provided a distinctive chiral-label-free SERS-based strategy to identify small aromatic chiral compounds with simplicity, feasibility and versatility. Our chiral sensing strategy has exhibited excellent discrimination performance for both enantioselectivity and chiral molecular fingerprint specificity with no need for any chiral auxiliary or circularly polarized light. Our strategy has tremendous potential for application in more sophisticated systems to realize the recognition among different chiral molecules.

Results and Discussion

The chiral discrimination sensing system was constituted by the mixed-thiol-functionalized Au NRs arrays, which were fabricated by an evaporation-induced assembly method (see the Supporting Information for the detailed procedure and characterization). Au NRs with different lengths and the

aspect ratios possess different surface plasma resonance (SPR) bands, especially the longitudinal SPR bands, which produced different EM enhancements. Considering this shape-dependent optical characteristics of Au NRs, we synthesized three kinds of Au NRs with distinctive longitudinal SPR bands from 715 to 780 and 835 nm (Supporting Information, Figure S1) to construct different vertically aligned Au NRs arrays. The prepared Au NRs arrays were vertically aligned into a monolayer and possessed a high degree of pattern regularity, as shown in the Supporting Information, Figure S2. To evaluate the enhancement performance of these prepared Au NRs arrays, SERS experiments with a rhodamine 6G (R6G) molecule as the probe were carried out. With the comparison of the SERS spectra of R6G adsorbed on three different assembled Au NRs arrays substrates, it was observed that the vertically aligned arrays composed of Au NRs with the longitudinal SPR bands at 780 nm engendered the strongest EM field and the largest SERS enhancement at the laser excitation wavelength of 785 nm, as shown in the Supporting Information, Figure S3. Thus, the Au NRs with an aspect ratio of about 3.8 and the longitudinal SPR bands at 780 nm to fabricate the Au NRs arrays substrate were used in the subsequent SERS experiments. Such Au NRs arrays displayed a good SERS enhancement for improving the molecular specific determination, and the remarkable uniformity and reproducibility to afford reliable determination results (Supporting Information, Figures S4 and S5).

By modifying the surface of the assembled Au NRs arrays with the mixed-thiol SAMs, composed of HT and MPBA, a chiral discrimination sensing platform was established, as illustrated in Figure 1. Considering the great influence that the ordering of the thiol SAMs has on the non-specific binding of the target molecules, SERS experiments were conducted to investigate the correlation between the soak time of HT and the molecular ordering. Aiming to obtain ordered HT assembly and high capture capability for chiral molecules, the soaking time of the vertically aligned Au NRs arrays was optimized (see the Supporting Information for the details and Figure S6). The immersion time was chosen to be 6 h for the subsequent SERS experiments, where the intensity

ratio of the HT bands at 628 and 698 cm^{-1} , attributed to the *gauche* ($\nu_{(\text{C-S})\text{G}}$) and *trans* ($\nu_{(\text{C-S})\text{T}}$) conformations of the S-C-C chain, respectively, were used to judge the degree of ordering of the thiol SAMs.^[38,39] After modifying a layer of HT, the Au NRs arrays were further soaked in the MPBA solution for another 6 h to generate mixed-thiol SAMs consisting of HT and MPBA. Unlike the aromatic MPBA, HT does not contain conjugated π -electrons; therefore, the SERS signal intensity of HT is lower than that of MPBA, even when the concentration of HT is larger and its acquisition time is longer than that of MPBA (Supporting Information, Figure S7).^[30] Since MPBA possessed the dominant SERS signal in the mixed-thiol SAMs, its concentration is vital for maximizing the enantioselective sensitivity and determining the chiral molecular fingerprint specificity without the interference of MPBA molecules. After investigating SERS spectra of the mixed thiols adsorbed onto the Au NRs arrays with varying concentrations of MPBA of 10^{-5} , 10^{-4} , and 10^{-3} M (Figure S8; see the Supporting Information for detailed discussion), the mixed-thiol SAMs prepared with 10^{-4} M MPBA was chosen for fabricating the chiral discrimination sensing platform. With this concentration, both MPBA and HT exhibited appropriate SERS signal intensities, which are necessary for the chiral discrimination with excellent enantioselectivity and high molecular fingerprint specificity. The enantioselectivity would be observed from the changes in the SERS spectra of MPBA, which originate from the intermolecular interactions between MPBA and the chiral target molecules.^[40,41] On the other hand, the high molecular fingerprint specificity is dependent on the capture ability of HT. This involves HT pulling the chiral targets into the hot spot regions of the vertically aligned Au NRs arrays, which can engender tremendous SERS signal enhancement that assists in determining the characteristic information about molecules. In addition, the mixed-thiol-functionalized Au NRs arrays prepared with such a method remained achiral (Supporting Information, Figure S9).

The prepared chiral discrimination sensing platform was then soaked in 10^{-3} M enantiomeric solutions of L- and D-mandelic acid (MA) for 12 h, separately. SERS spectra of the chiral discrimination sensing systems with the different enantiomeric targets were collected after rinsing and drying, as shown in Figure 2A. Even though the MA enantiomers were diluted to 10^{-3} M, rather than pure liquid solution, the SERS-based chiral discrimination method still demonstrated a distinct enantioselective discrepancy and a fairly good detection performance for the molecular specificity of MA. For comparison, all the SERS spectra acquired were normalized by the strongest band of MPBA at 1075 cm^{-1} , in consideration of its insensitivity to the surroundings.^[30,42] It can be observed that obvious spectral changes occurred between the SERS spectrum of the blank chiral discrimination sensing platform and those systems with different MA enantiomers. Several bands appeared at 358, 473, 1168, and 1239 cm^{-1} after introducing the L- and D-MA enantiomers into the system (Figure 2A, b and c),^[43] which belong to neither MPBA nor HT. These emerging bands coincide with the extra bands in the SERS spectrum of the Au NRs arrays substrate that was modified with only HT after immersion

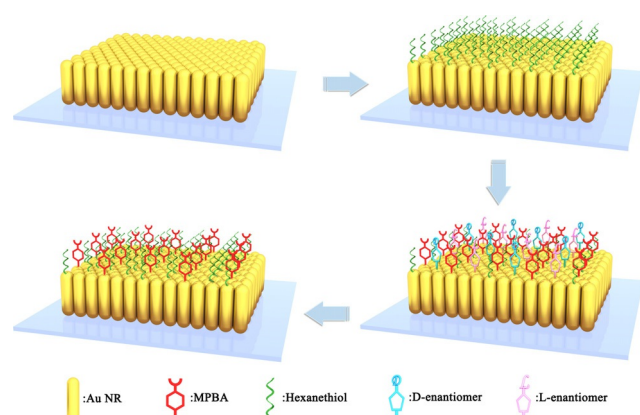


Figure 1. Illustration of preparation of the chiral sensing recognition system.

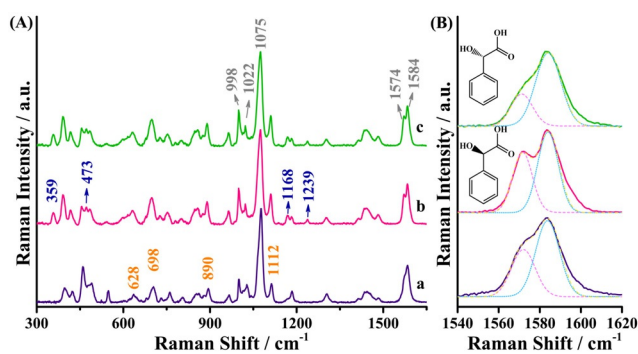


Figure 2. A) SERS spectra of a) the blank chiral discrimination sensing platform, and the chiral discrimination sensing system with the incorporation of b) D-MA and c) L-MA. B) Enlargements of the 1540–1620 cm^{-1} region of the SERS spectra shown in (A). All the SERS spectra were normalized by the intensity of the band at 1075 cm^{-1} .

with MA (Supporting Information, Figure S10, b and c), and are attributed to MA as they also coincide with the characteristic Raman bands of MA (Supporting Information, Figure S10, a).

An obvious difference in the relative intensity of the two bands at 1574 and 1584 cm^{-1} , attributed to the C=C stretching vibration modes of MPBA, between the L- and D-MA enantiomeric systems can be recognized, as shown in Figure 2B. When L-MA was involved in the chiral discrimination system, the band at 1574 cm^{-1} , arising from the B-C stretching coupled with the non-totally symmetric stretching ($\nu_{\text{C-C}}$, b_2) mode of MPBA, is much weaker than the band at 1584 cm^{-1} (the totally symmetric stretching vibration, a_1 mode), as shown in Figure 2B, c. The intensity of the b_2 mode at 1574 cm^{-1} is significantly lower than that of the corresponding band of the blank chiral discrimination sensing platform (Figure 2B, a). Unlike the L-MA discrimination sensing system, the intensity of the b_2 mode in the D-MA discrimination system markedly increases and exhibits an obvious shoulder peak with respect to the a_1 mode of MPBA (Figure 2B, b). It is of note that the difference in the relative intensities of the b_2 mode and the a_1 mode are dependent on the chiral environment of the system, as revealed from the SERS spectra. Changes in the b_2 modes in the SERS spectra of molecules with C_{2v} symmetry can be regarded as evidence for the occurrence of CT processes;^[44,45] therefore, the excellent enantioselectivity is closely associated with the differentiated CT processes in different chiral discrimination sensing systems.

A possible sensing mechanism of the SERS-based discrimination sensing system toward the L-/D-MA enantiomers is extremely important for understanding this discrimination process. The results in Figure 2 reveal that the discrimination sensing system possesses not only great enantioselectivity but also high-resolution molecular fingerprint specificity. Regarding the enantioselectivity, the distinction between the L- and D-MA enantiomers manifests from the different relative intensities of the MPBA bands in the SERS spectra. The intermolecular hydrogen bonding between the L- or D-MA enantiomers and MPBA accounts for the enantioselectivity of the sensing system. As we previously reported,^[46,47] hydrogen

bonding interactions result in the rearrangement of the electron density of a self-assembled system. They alter the molecular electronic structure (as shown in the Supporting Information, Figure S11) and further influence the CT process between a metal substrate and its adsorbates, which engenders the distinguishable SERS spectral patterns of the adsorbed probes. Different hydrogen bonding interactions should take place in the two enantiomeric systems, occurring between the carboxyl group of MA and the hydroxyl group of MPBA and leading to different CT processes in the system that involve discrepant CT states.^[46,48] Since CT is one of the main enhancers of SERS, any subtle change in the CT states would cause a change in the SERS spectral patterns.^[25,49] The intensities of b_2 and a_1 modes in the SERS spectra can be used to evaluate the occurrence and degree of the CT process in the discrimination sensing system.^[50,51] When L-MA is introduced into the discrimination sensing system, the b_2 mode of MPBA decreases with respect to the blank system. However, the b_2 mode shows visible enhancement in the presence of D-MA. Thus, it can be concluded that the enantioselectivity of the system is strongly associated with the CT process.^[25] The CT-based SERS, in turn, amplifies the subtle differences between the two enantiomeric sensing systems caused by chirality in comparison to the discrimination method with the use of circular dichroism (Supporting Information, Figure S12).

The molecular specificity of MA of this sensing system benefits from the advantages of Raman spectroscopy, which can afford specific molecular fingerprint information to identify and quantify analytes with high sensitivity.^[16] In the course of chiral discrimination sensing, determining molecular fingerprint information was parallel to recognizing the chirality. Therefore, MA was prone to determination despite the relatively low molecular concentration used. This was confirmed by the characteristic Raman bands of MA appearing at 359, 473, 1168, and 1239 cm^{-1} (Figure 2). The sensitivity is due to the huge enhancement of the SERS signal, which primarily originates from the enormous plasmonic near-field enhancement from the nanosized metal substrates.^[19,52] The vertically aligned Au NRs arrays that we fabricated as SERS substrates for our chiral discrimination sensing system have been shown to produce a strong SPR effect and generate a strong and homogeneous EM field, especially in the hot spot regions located between two adjacent rods.^[34,37] It can be considered that the molecular specificity of MA is largely determined by the EM mechanism of SERS and the trapping ability of the achiral captor HT. Even though the Au NRs arrays provide a huge enhancement, the low affinity between the target molecule and the Au NRs array substrate still severely restricts the detection sensitivity in SERS spectroscopy. However, the HT component in the mixed-thiol SAMs effectively addresses this issue by forming non-specific intermolecular interactions between HT and the target chiral molecules.

A suggested chiral discrimination mechanism was proposed and is illustrated in Figure 3. In the discrimination process, we suggest that L- or D-MA enantiomers containing hydrophobic aromatic ring are prone to be pulled into the mixed-thiol SAMs by HT via van der Waals and hydrophobic

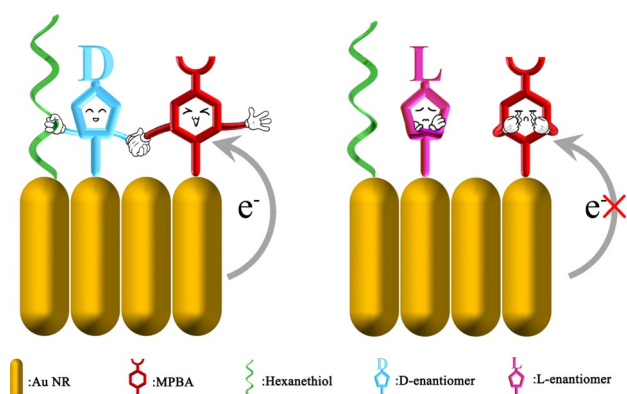


Figure 3. A representation showing interactions of the sensing platform with D- and L-MA enantiomers and the enantioselective discrimination process.

interactions.^[53] In such a case, the L- or D-MA enantiomers are situated in the hot spot regions of the vertically aligned Au NRs arrays, and are sensitively detected due to the tremendous EM enhancement. On the other hand, the hydrophilic carboxyl and hydroxyl groups of the MA enantiomers remain outside of the alkane chain of HT and interact with the hydroxyl group of the adjacent MPBA through hydrogen bonding. This causes the differentiated electronic structures of the Au-MPBA complexes and CT processes, giving the distinctive SERS spectra of the two enantiomeric systems. The b_2 mode of MPBA decreases with L-MA present, indicating unfavorable intermolecular hydrogen bonding geometries form between L-MA and MPBA, which generate CT-states that may not be suitable for the CT from the Au NRs to MPBA. As for the discrimination system with D-MA present, the b_2 mode of MPBA is visibly enhanced, manifesting the formation of favorable hydrogen bonding geometries that promote the CT processes in this system between D-MA and MPBA.

As a conventional achiral chemical-capturing molecule, MPBA undergoes pH-dependent structural changes,^[54,55] which produces different SERS spectral patterns of MPBA under different pH conditions (Supporting Information, Figure S13A). It is necessary to investigate the SERS spectra of the mixed-thiol SAMs on the Au NRs arrays in solution at pH levels ranging from 1 to 13 to elucidate at which pH the chiral discrimination sensing system displays optimal discrimination performance. The SERS spectra presented in the Supporting Information, Figure S13B show that the a_1 mode of MPBA at 1584 cm^{-1} is evidently stronger than the b_2 mode at 1574 cm^{-1} under acidic conditions ($\text{pH} \leq 6$). Gradually, as pH increases, the b_2 mode increases and the a_1 mode decreases until the intensities of the two modes are reversed at alkaline pH values ($\text{pH} \geq 9$). The variations in MPBA SERS spectra can be attributed to its molecular configuration in alkaline pH environments. When the surrounding pH is acid, the B atom in MPBA is sp^2 -hybridized with a triangular planar configuration, but is sp^3 -hybridized under alkaline pH conditions by forming an (OH^-) -MPBA anion with a tetrahedral configuration.^[55] These pH-determined configuration changes prompt a symmetry-reduction-induced decrease in

the degeneracy of the energy levels in MPBA, accompanied by charge redistributions of its benzene ring in the MPBA molecule, which consequently affect the CT process between the Fermi level of Au and the molecular orbital level of MPBA. Therefore, the intensities of C=C stretching vibrations of the benzene distinctly change.

The discrimination behavior of our sensing system was subsequently investigated by SERS with pH conditions ranging from 1 to 13 (Figure 4). The individual comparisons of the chiral discrimination behavior under each pH condition are presented in the Supporting Information, Figure S14. Increasing the pH of the system enhances its discrimination capability, and the discrepancies between the SERS spectra of the L- and D-MA systems increase. We found the optimized pH condition for this system to be an alkaline pH of 9. At this pH, the spectral discrepancies in the relative intensities of the b_2 and a_1 modes between the L- and D-MA sensing systems are remarkable, and excellent enantioselectivity is exhibited, although the maximum differentiation between the two enantiomeric systems was not achieved. In addition, the alkalinity is comparatively mild at pH 9, where the assembled vertically aligned Au NRs arrays are stable. On this account, the following SERS experiments were performed at a pH of 9 to obtain optimal spectral discriminability. To examine the enantioselectivity of the system, MA enantiomeric solutions with various enantiomeric excess (ee) values were investigated (Figure 5A). The relative intensity ratio of the b_2 to a_1 modes of MPBA (I_{1574}/I_{1584}), as an enantioselective indicator, decreased with increasing ee % values of L-MA, which

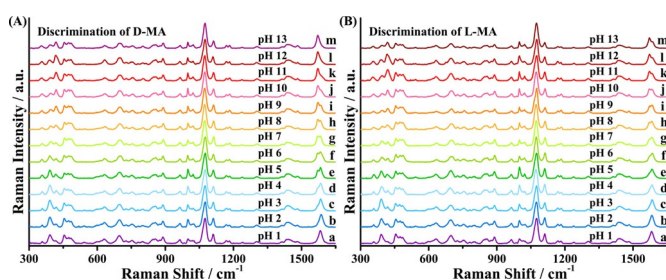


Figure 4. SERS discrimination performance of the chiral discrimination system for A) D-MA and B) L-MA enantiomers under different pH conditions ranging from 1 to 13 (from a to m). All the SERS spectra were normalized by the intensity of the band at 1075 cm^{-1} .

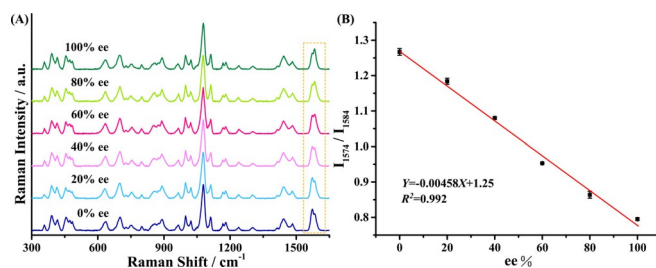


Figure 5. A) SERS spectra of the chiral discrimination system for the discrimination of enantiomer with various ee value of L-MA. B) Correlation between the differences in the relative intensity ratio of I_{1574}/I_{1584} and the ee values (in %). All the SERS spectra were normalized by the intensity of the band at 1075 cm^{-1} .

revealed a linear correlation with an $R^2 = 0.992$ (Figure 5B). It indicates that the chiral discrimination sensing system exhibits the impressed enantioselectivity.

Other crucial factors that affect the chiral discrimination performance are the component and structure of the achiral mixed-thiol SAMs on the assembled Au NRs arrays. The HT fraction of the mixed-thiol SAMs determines its ability to provide molecular fingerprint specificity, as evidenced by the control experiment where only MPBA was used to fabricate a single-thiol SAMs. However, the characteristic SERS signals of MA were negligible in the SERS spectra of the system containing the MPBA-only SAMs, despite the spectral differences and the good enantioselectivity obtained between the L- and D-MA (Figure S15). This shows that the cooperative effects of the mixed thiols, HT and MPBA, in the sensing system afford the excellent chiral discrimination performance. Since the molecular heights of the assembled HT and MPBA are similar,^[30] synergetic properties produce owing to the exposure of the functional groups of each modifier. As a consequence, the mixed-thiol SAMs make the chiral targets to be captured by HT and recognized by the adjacent MPBA with extremely high enantioselectivity and molecular specificity. To further verify this, we fabricated three other chiral discrimination sensing systems by replacing HT with other alkylthiols: 1-octanethiol (OT), 1-decanethiol (DT) and 1-octadecanethiol (ODT). We examined the chiral discrimination performance of three mixed-thiol SAMs at a pH of 9 (Supporting Information, Figure S16). All three systems exhibited almost the same enantioselectivity as the original discrimination system for L- and D-MA, which is because distinguishing between the two enantiomers relies heavily on their interaction with MPBA. With respect to molecular specificity, the distinct fingerprint characteristic bands of MA, located at 359, 473, 1168, and 1239 cm^{-1} , can be detected only in the discrimination system with HT and MPBA. In the discrimination sensing system fabricated with OT and MPBA, only faint SERS signals of MA could be identified (Supporting Information, Figure S16B), while the characteristic bands of MA were negligible in the SERS spectra of the other two discrimination systems (Supporting Information, Figure S16C,D). A conclusion has been thus drawn from these results that the similar height of the mixed thiols is of great importance to trap the chiral targets into the hot spot regions of the Au NRs arrays and offer the molecular specificity.

Since the microstructure of the two modifiers is vital in determining the synergistic properties of the mixed-thiol SAMs, alkylthiols with identical carbon chain lengths but different terminal functional groups were chosen to demonstrate the effect of the terminal groups on the determination capability of the sensing system. The van der Waals and hydrophobic interactions are the main driving forces for HT to anchor the chiral target molecules onto the Au NRs surface. Further evidence was presented using 6-mercapto-1-hexanol (MCH) and 6-mercaptohexanoic acid (MHA), thiols with hydrophilic hydroxyl and carboxyl terminal group, respectively, to replace HT when forming the mixed-thiol SAMs. The detection abilities of these sensing systems for MA reduce as the hydrophobicity of the alkylthiols decrease,

as shown in the Supporting Information, Figure S17. The MA molecules can be determined only in the chiral discrimination system formed by HT and MPBA. The results from the SERS detection in these three sensing systems indicate that the hydrophobic interaction is crucial for the detection of chiral molecules with high specificity.

The remarkable chiral discrimination capability of this SERS-based sensing system encouraged us to attempt the recognition of a variety of small aromatic molecules, most of which are components of numerous chiral pharmaceuticals. Under the optimized conditions, the discrimination sensing system exhibited an amazing response to these chiral aromatic molecules with pronounced spectral enantioselectivity between the two enantiomers and significant molecular specificity. As displayed in Figure 6, another ten chiral aromatic molecules, including phenylalanine (Phe), phenylalaninol (PhA), phenylglycinol (PGI), α -phenylglycine (PGe), phenylethanol (PEt), 1-phenyl-1-propanol (PhP), phenyllactic acid (PLA), α -phenethylamine (PEa), 1,2,3,4-Tetrahydro-1-naphthylamine (THNA), and hydroxyphenylglycine (HPG), were recognized with comparable or even superior enantioselectivity and molecular specificity to that of MA molecule. In these discrimination sensing systems, the b_2 mode of MPBA was visibly enhanced when the system underwent incubation with D (or R)-type enantiomers, but an intense decrease in its intensity was observed when the system

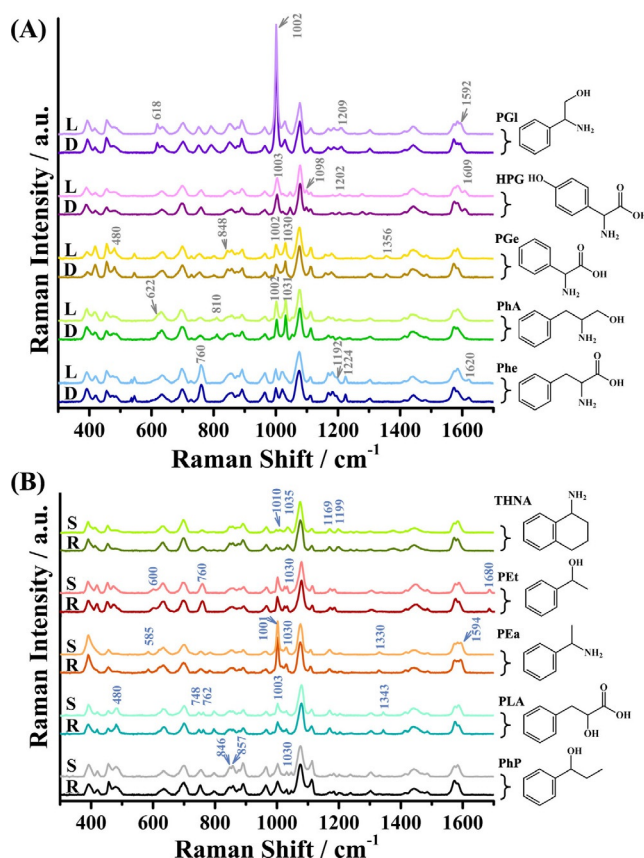


Figure 6. SERS spectra of the chiral discrimination sensing system for the discrimination of other ten kinds of chiral aromatic molecules A) Phe, PhA, PGe, HPG, PGI, and B) PhP, PLA, PEa, PEt, and THNA.

involved L (or S)-type enantiomers. Aside from the arresting spectral discrepancies of the relative intensities of the b_2 and a_1 modes of MPBA, the molecular structure information of each chiral target was also effectively identified, which enabled target chiral to be distinguished among diverse chiral molecules. Consequently, this SERS-based chiral discrimination sensing system possesses versatility for recognizing a variety of chiral aromatic molecules.

Conclusion

A chiral-label-free and versatile chiral discrimination sensing system has been developed based on the vertically aligned Au NRs arrays modified with the achiral mixed-thiol SAMs using SERS spectroscopy to differentiate and identify small aromatic molecules in solution. The key to success in chiral discrimination for this strategy is attributed to the synergy of the CT contribution and the EM enhancement of SERS. The chiral discrepancy between L- and D-enantiomers is identified from the distinct differences in the SERS spectral intensities, which are dependent on the MPBA fraction of the mixed-thiols SAMs. A suggested mechanism toward this impressive enantioselective recognition was presented considering the relevance between the enantioselectivity and CT enhancement of SERS on account of the differentiated SERS relative intensities of MPBA. Additionally, a linear correlation was obtained between the relative intensity ratio of the b_2 and a_1 modes of the SERS spectra of MPBA and *ee* % values under the optimal conditions at pH 9. The unique fingerprint characteristics of the target chiral molecules can be detected with extremely high molecular specificity owing to the capture ability of the HT fraction of the mixed-thiol SAMs, which traps the chiral molecules in the hot spot regions of the vertically aligned Au NRs arrays with non-specific intermolecular interactions and exposes them to an enhanced EM field. This SERS-based chiral discrimination sensing system has demonstrated excellent versatility for various chiral aromatic molecules, which could be promising for applications in identifying diverse chiral compounds in sophisticated systems. We believe this work provides a robust and simple strategy for the discrimination and detection of chiral molecules in various fields, such as asymmetric synthesis, chiral catalysis and enantiomeric separation.

Acknowledgements

This work was supported by the National Natural Science Foundation of China (NSFC, 21705015, 61705227, 21675020, and 21773080), the Fundamental Research Funds for the Central Universities (N2005020), the Development Program of the Science and Technology of Jilin Province (20200201086JC, 20190701003GH) and the Open Project of State Key Laboratory of Supramolecular Structure and Materials (sklssm 202028).

Conflict of interest

The authors declare no conflict of interest.

Keywords: charge transfer · small aromatic molecules · SERS · chiral discrimination

- [1] N. Gao, Z. Du, Y. Guan, K. Dong, J. Ren, X. Qu, *J. Am. Chem. Soc.* **2019**, *141*, 6915–6921.
- [2] F. Zaera, *Chem. Soc. Rev.* **2017**, *46*, 7374–7398.
- [3] D. P. Glavin, A. S. Burton, J. E. Elsil, J. C. Aponte, J. P. Dworkin, *Chem. Rev.* **2019**, <https://doi.org/10.1021/acs.chemrev.9b00474>.
- [4] T. J. Wenzel, *Differentiation of Enantiomers, Vol. 1* (Eds.: V. Schurig), Springer, Heidelberg, **2013**, pp. 1–68.
- [5] Z. Han, K. Wang, Y. Guo, W. Chen, J. Zhang, X. Zhang, G. Siligardi, S. Yang, Z. Zhou, P. Sun, W. Shi, P. Cheng, *Nat. Commun.* **2019**, *10*, 5117.
- [6] K. W. Bentley, Y. G. Nam, J. M. Murphy, C. Wolf, *J. Am. Chem. Soc.* **2013**, *135*, 18052–18055.
- [7] H. He, K. Zhao, L. Xiao, Y. Zhang, Y. Cheng, S. Wan, S. Chen, L. Zhang, X. Zhou, K. Liu, H. Zhang, *Angew. Chem. Int. Ed.* **2019**, *58*, 18286–18289; *Angew. Chem.* **2019**, *131*, 18454–18457.
- [8] X. Zhang, J. Yin, J. Yoon, *Chem. Rev.* **2014**, *114*, 4918–4959.
- [9] T. A. Keiderling, *Chem. Rev.* **2020**, <https://doi.org/10.1021/acs.chemrev.1029b00636>.
- [10] X. Gao, B. Han, X. Yang, Z. Tang, *J. Am. Chem. Soc.* **2019**, *141*, 13700–13707.
- [11] D. Wu, J. Yang, Y. Peng, Y. Yu, J. Zhang, L. Guo, Y. Kong, J. Jiang, *Sens. Actuators B* **2019**, *282*, 164–170.
- [12] P. Lesot, C. Aroulanda, H. Zimmermann, Z. Luz, *Chem. Soc. Rev.* **2015**, *44*, 2330–2375.
- [13] M. Lämmerhofer, *J. Chromatogr. A* **2010**, *1217*, 814–856.
- [14] T. Nakakoji, H. Sato, D. Ono, H. Miyake, S. Shinoda, H. Tsukube, H. Kawasaki, R. Arakawa, M. Shizuma, *Chem. Commun.* **2020**, *56*, 54–57.
- [15] Y. Wang, Z. Yu, W. Ji, Y. Tanaka, H. Sui, B. Zhao, Y. Ozaki, *Angew. Chem. Int. Ed.* **2014**, *53*, 13866–13870; *Angew. Chem.* **2014**, *126*, 14086–14090.
- [16] S. Schlücker, *Angew. Chem. Int. Ed.* **2014**, *53*, 4756–4795; *Angew. Chem.* **2014**, *126*, 4852–4894.
- [17] K. Kneipp, Y. Ozaki, Z. Q. Tian, *Recent Developments in Plasmon-Supported Raman Spectroscopy*, World Scientific Publishing Europe Ltd., London, **2018**, pp. 255–298.
- [18] K. A. Willets, R. P. Van Duyne, *Annu. Rev. Phys. Chem.* **2007**, *58*, 267–297.
- [19] S. Y. Ding, E. M. You, Z. Q. Tian, M. Moskovits, *Chem. Soc. Rev.* **2017**, *46*, 4042–4076.
- [20] J. R. Lombardi, R. L. Birke, *Acc. Chem. Res.* **2009**, *42*, 734–742.
- [21] I. Alessandri, J. R. Lombardi, *Chem. Rev.* **2016**, *116*, 14921–14981.
- [22] Y. Wang, J. Liu, Y. Ozaki, Z. Xu, B. Zhao, *Angew. Chem. Int. Ed.* **2019**, *58*, 8172–8176; *Angew. Chem.* **2019**, *131*, 8256–8260.
- [23] X. Wang, P. Li, X. X. Han, Y. Kitahama, B. Zhao, Y. Ozaki, *Nanoscale* **2017**, *9*, 15303–15313.
- [24] Y. Wang, J. Liu, X. Zhao, C. Yang, Y. Ozaki, Z. Xu, B. Zhao, Z. Yu, *Chem. Commun.* **2019**, *55*, 9697–9700.
- [25] Y. Wang, Z. Yu, X. Han, H. Su, W. Ji, Q. Cong, B. Zhao, Y. Ozaki, *J. Phys. Chem. C* **2016**, *120*, 29374–29381.
- [26] C. Vericat, M. E. Vela, G. Benitez, P. Carro, R. C. Salvarezza, *Chem. Soc. Rev.* **2010**, *39*, 1805–1834.
- [27] H. Häkkinen, *Nat. Chem.* **2012**, *4*, 443–455.
- [28] A. Stewart, S. Zheng, M. R. McCourt, S. E. J. Bell, *ACS Nano* **2012**, *6*, 3718–3726.
- [29] T. Schmaltz, G. Sforazzini, T. Reichert, H. Frauenrath, *Adv. Mater.* **2017**, *29*, 1605286.

- [30] F. Sun, J. R. E. Menye, D. D. Galvan, T. Bai, H. C. Hung, Y. N. Chou, P. Zhang, S. Jiang, Q. Yu, *ACS Nano* **2015**, *9*, 2668–2676.
- [31] E. Pfitzner, H. Seki, R. Schlesinger, K. Ataka, J. Heberle, *ACS Sens.* **2018**, *3*, 984–991.
- [32] S. Bandyopadhyay, S. Chattopadhyay, A. Dey, *Phys. Chem. Chem. Phys.* **2015**, *17*, 24866–24873.
- [33] M. C. R. González, A. G. Orive, P. Carro, R. C. Salvarezza, A. H. Creus, *J. Phys. Chem. C* **2014**, *118*, 30013–30022.
- [34] J. Reguera, J. Langer, D. Jimenez de Aberasturi, L. M. Liz-Marzan, *Chem. Soc. Rev.* **2017**, *46*, 3866–3885.
- [35] M. Mao, B. Zhou, X. Tang, C. Chen, M. Ge, P. Li, X. Huang, L. Yang, J. Liu, *Chem. Eur. J.* **2018**, *24*, 4094–4102.
- [36] P. Li, Y. Li, Z. K. Zhou, S. Tang, X. F. Yu, S. Xiao, Z. Wu, Q. Xiao, Y. Zhao, H. Wang, P. K. Chu, *Adv. Mater.* **2016**, *28*, 2511–2517.
- [37] B. Peng, G. Li, D. Li, S. Dodson, Q. Zhang, J. Zhang, Y. H. Lee, H. V. Demir, X. Y. Ling, Q. Xiong, *ACS Nano* **2013**, *7*, 5993–6000.
- [38] C. E. Taylor, M. H. Schoenfish, J. E. Pemberton, *Langmuir* **2000**, *16*, 2902–2906.
- [39] M. H. Schoenfish, J. E. Pemberton, *J. Am. Chem. Soc.* **1998**, *120*, 4502–4513.
- [40] D. Li, Y. Chen, Z. Liu, *Chem. Soc. Rev.* **2015**, *44*, 8097–8123.
- [41] J. Müller, R. A. Kirschner, A. Geyer, G. Klebe, *ACS Omega* **2019**, *4*, 775–784.
- [42] F. Sun, T. Bai, L. Zhang, J. R. Ella-Menye, S. Liu, A. K. Nowinski, S. Jiang, Q. Yu, *Anal. Chem.* **2014**, *86*, 2387–2394.
- [43] H. M. Badawi, W. Forner, *Spectrochim. Acta Part A* **2011**, *78*, 1162–1167.
- [44] S. P. Centeno, I. López-Tocón, J. Roman-Perez, J. F. Arenas, J. Soto, J. C. Otero, *J. Phys. Chem. C* **2012**, *116*, 23639–23645.
- [45] J. R. Lombardi, R. L. Birke, *J. Phys. Chem. C* **2008**, *112*, 5605–5617.
- [46] Y. Wang, W. Ji, H. Sui, Y. Kitahama, W. Ruan, Y. Ozaki, B. Zhao, *J. Phys. Chem. C* **2014**, *118*, 10191–10197.
- [47] Y. Wang, W. Ji, Z. Yu, R. Li, X. Wang, W. Song, W. Ruan, B. Zhao, Y. Ozaki, *Phys. Chem. Chem. Phys.* **2014**, *16*, 3153–3161.
- [48] W. Xi, B. K. Shrestha, A. J. Haes, *Anal. Chem.* **2018**, *90*, 128–143.
- [49] F. Avila, D. J. Fernandez, J. F. Arenas, J. C. Otero, J. Soto, *Chem. Commun.* **2011**, *47*, 4210–4212.
- [50] K. Ikeda, S. Suzuki, K. Uosaki, *J. Am. Chem. Soc.* **2013**, *135*, 17387–17392.
- [51] J. Chowdhury, *Appl. Spectrosc. Rev.* **2015**, *50*, 240–260.
- [52] S. Ding, J. Yi, J. Li, B. Ren, D. Wu, R. Panneerselvam, Z. Tian, *Nat. Rev. Mater.* **2016**, *1*, 16021.
- [53] D. Grumelli, L. P. Mendez De Leo, C. Bonazzola, V. Zamlynny, E. J. Calvo, R. C. Salvarezza, *Langmuir* **2010**, *26*, 8226–8232.
- [54] P. Yan, Z. Ding, X. Li, Y. Dong, T. Fu, Y. Wu, *Anal. Chem.* **2019**, *91*, 12134–12137.
- [55] L. Su, T. Chen, T. Xue, A. Sheng, L. Cheng, J. Zhang, *ACS Appl. Mater. Interfaces* **2020**, *12*, 7650–7657.

Manuscript received: May 31, 2020

Revised manuscript received: July 20, 2020

Accepted manuscript online: July 29, 2020

Version of record online: September 9, 2020